Proc. of SPIE Medical Imaging: Visualization, Image-guided Procedures, and Modeling, vol. 6918, 69180Q, 2008.

Image-based mass-spring model of mitral valve closure for surgical planning

Peter E. Hammer*[a,b], Douglas P. Perrin[b], Pedro J. del Nido[b], Robert D. Howe[c]

[a]Department of Biomedical Engineering, Tufts University, Medford, MA, [b]Department of Cardiac Surgery, Children's Hospital, Boston, MA, [c]School of Engineering and Applied Sciences, Harvard University, Cambridge, MA

ABSTRACT

Surgical repair of the mitral valve is preferred in most cases over valve replacement, but replacement is often performed instead due to the technical difficulty of repair. A surgical planning system based on patient-specific medical images that allows surgeons to simulate and compare potential repair strategies could greatly improve surgical outcomes. In such a surgical simulator, the mathematical model of mechanics used to close the valve must be able to compute the closed state quickly and to handle the complex boundary conditions imposed by the chords that tether the valve leaflets. We have developed a system for generating a triangulated mesh of the valve surface from volumetric image data of the opened valve. We then compute the closed position of the mesh using a mass-spring model of dynamics. The triangulated mesh is produced by fitting an isosurface to the volumetric image data, and boundary conditions, including the valve annulus and chord endpoints, are identified in the image data using a graphical user interface. In the mass-spring model, triangle sides are treated as linear springs, and sides shared by two triangles are treated as bending springs. Chords are treated as nonlinear springs, and self-collisions are detected and resolved. Equations of motion are solved using implicit numerical integration. Accuracy was assessed by comparison of model results with an image of the same valve taken in the closed state. The model exhibited rapid valve closure and was able to reproduce important features of the closed valve.

Keywords: mitral valve, mass-spring model, simulation

1. INTRODUCTION

The valves of the human heart ensure one way blood flow and play a critical role in normal heart function. A malfunctioning valve can either hinder forward flow or allow retrograde flow, both of which can over-work the heart and lead to heart failure. More than 130,000 surgeries are performed each year in the United States to treat malfunctioning or diseased heart valves [6]. Over 42,000 of those surgeries are performed on the mitral valve [11], a complex structure consisting of two leaflets tethered by fibrous chordae tendinae (chords) to the papillary muscles on the ventricular wall (Fig. 1). The two primary surgical treatment options for a malfunctioning mitral valve are repair of the native mitral valve tissue and replacement of the valve with a mechanical or bioprosthetic valve. Repair has been shown to result in better function and long-term survival than replacement [10,15,19]. In fact, the American College of Cardiology and the American Heart Association recommend mitral valve repair over replacement whenever adequate surgical skill is available [3].

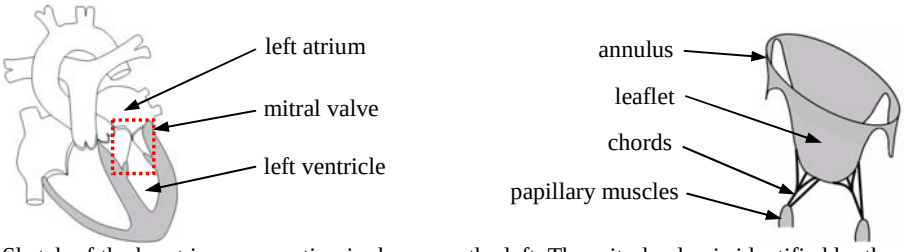

Figure 1. Sketch of the heart in cross-section is shown on the left. The mitral valve is identified by the red (dotted) box. A sketch of the mitral valve and its main structures is shown on the right.

* peter.hammer@childrens.harvard.edu; phone 1 617 919-2317

Despite these studies and recommendations, valve replacement is often performed due to the technical difficulty of repair. Repairs are typically performed when the patient is on cardiopulmonary bypass, when the heart has been emptied of blood and is not beating. It is difficult for the surgeon to predict how potential repair strategies will translate into valve function after the heart is closed, refilled with blood and allowed to resume beating. For example, the surgeon must often decide how much tissue to cut out of an open valve leaflet to change the closed shape of the valve, or must decide what length and attachment point for a replacement chord will lead to effective valve closure. Studies show that experienced surgeons at large clinical centers have a much better record of successful repairs, and valve replacement is often chosen instead of repair at low volume centers [9].

A surgical simulation environment could provide a valuable tool to help the surgeon plan a surgical repair strategy and could potentially improve the success rate for mitral valve repair. Ideally, such a simulator would be based on pre-operative, patient-specific clinical images. It would allow the surgeon to interact with a computer model of the valve in the open state – the same state the valve is in during surgery. The surgeon would be able to make surgical modifications to the leaflets and chords of the model, and a model of mechanics would compute the closed state of the valve and predict competency of the modified valve. This could be done for many surgical repair strategies, allowing the surgeon to select an optimum approach before surgery.

A crucial component in such a surgical simulator is the mechanical model of the valve. Many groups have developed computational models of mitral valve mechanics. Finite element modeling has been used to study specific aspects of mitral valve function [7,13,20]. For these studies, valve geometry was based on averaged valve data, and leaflets were assumed to be symmetrical through their midlines. Another finite element study modeled the valve structures asymmetrically and obtained boundary conditions dynamically from sonomicromety crystals implanted in an animal model [14]. The finite element modeling methods used in these studies, however, are not based on clinical imaging methods and do not execute at speeds fast enough for use in a pre-surgical planning system.

To meet these requirements, we have developed a computational model based on a mass-spring system, a method that is commonly used in computer graphics to simulate the dynamics of fabric [16]. Mitral valve geometry is read directly from computed tomography (CT) data, and this data is used to generate a triangular mesh. The mesh is treated as a system of translational and bending springs, and simple dynamics are used to evolve the closed state of the valve. The closed state predicted by the model is compared directly with images of the actual valve taken in the closed state.

2. METHODS

2.1 Image acquisition

The mitral valve of an explanted porcine heart was statically loaded with air via tubing inserted through the aorta, past the aortic valve, and into the left ventricle. The aorta was then cinched tightly around the tubing. To prevent air leakage through the coronary arteries, they were sutured closed. In order to supply air at low pressure with high accuracy, a circuit consisting of low-pressure regulators and electronic pressure sensors was constructed. The heart was imaged in two different states using a micro-CT system (microCAT, Siemens, Munich, Germany): (1) with the mitral valve in the open position (no applied pressure), and (2) with the mitral valve in the closed position under typical porcine peak systolic pressure of 100 mmHg. Images were acquired at 100 μm isotropic voxel size.

2.2 Image processing

The volumetric CT image of the heart was first cropped to include only the structures of the mitral valve. A graphical user interface (GUI) was written in Matlab (Mathworks, Natick, MA) to allow image cropping through selection of an arbitrary region of interest through the individual image slices. The resulting image of the valve was segmented, and an isosurface was fit to the data in Matlab using a thresholding method. The surface consists of an unstructured triangular mesh of points covering all surfaces of the leaflets and chords. Another GUI was written to isolate the triangles comprising the atrial surface of the leaflets and to approximate all chords that attach to either the free edge or the belly of the leaflet with line segments.

2.3 Mass-spring model

2.3.1 Model structure

The dataset consisting of the triangulated mesh (representing the atrial surface of the leaflets) and line segments (representing the chords) was used as the basis for a mass-spring model. All sides of triangles were treated as translational springs, and every pair of triangles with a shared side was treated as a bending spring [8]. Vertices (nodes) lying on the mitral valve annulus were identified using semi-automated graphical tools, and these vertices were treated as a zero-displacement boundary condition. Spatial coordinates where chords insert into papillary muscle, connect to leaflets and possibly connect to one another were also identified, and each chord segment was treated as a translational spring whose spring constant becomes nonzero only when its length exceeds a length corresponding to the fully-extended, undeformed length of the chord. Furthermore, beyond a certain extension, chords no longer respond to elongation forces as described below in section 2.3.3. Nodal mass was computed as the product of the nodal area (one third of the sum of the areas of triangles sharing that node), leaflet thickness, and mass density.

2.3.2 Model dynamics

The dynamics of the system of masses can be expressed in state-space form as:

$$\begin{pmatrix} \dot{\vec{x}} \\ \dot{\vec{v}} \end{pmatrix} = \begin{pmatrix} \vec{v} \\ M^{-1}\vec{f} \end{pmatrix} \tag{1}$$

where x and v are vectors of nodal positions and velocities, respectively, M^{-1} is the inverse mass matrix (a diagonal matrix with the reciprocal of nodal mass on the main diagonal), and f is the vector of net nodal force due to all springs and external forces. This equation must be discretized for numerical solution, and a fundamental choice to be made is between explicit and implicit numerical integration methods. Explicit methods solve for the future (unknown) value of the state variables based entirely on past (known) values of the states. While simpler to implement, they are only conditionally stable. The condition for stability is that the time step be smaller than the time constant of the fastest modes of the system. In our case, the system is comprised of very small masses coupled by very stiff springs. The resulting time constants are very small requiring a correspondingly small integration time step and long solution time. Implicit methods, on the other hand, express the future (unknown) value of the state variables in terms of both past values as well as the unknown, future values of the states. These methods require simultaneous solution for all of the state variables at each time step. While this is more computationally intensive per time step than explicit integration, it is unconditionally stable, which allows larger integration step sizes [1]. With computational speed in mind, we pursued implicit integration for our model. Toward this end, we discretized equation 1 using a second-order backward-difference formula as:

$$\frac{1}{h}\begin{pmatrix} \frac{3}{2}\vec{x}^{n+1} - 2\vec{x}^{n} + \frac{1}{2}\vec{x}^{n-1} \\ \frac{3}{2}\vec{v}^{n+1} - 2\vec{v}^{n} + \frac{1}{2}\vec{v}^{n-1} \end{pmatrix} = \begin{pmatrix} \vec{v}^{n+1} \\ M^{-1}\vec{f}^{n+1} \end{pmatrix} \tag{2}$$

where h is the integration time step. The net nodal force at step $n+1$ depends on the nodal positions at step $n+1$ making the set of equations nonlinear. It can be linearized by replacing f at step $n+1$ with a first-order Taylor series approximation:

$$\vec{f}^{n+1} = \vec{f}^{n} + \frac{\partial \vec{f}}{\partial \vec{x}}\left(\vec{x}^{n+1} - \vec{x}^{n}\right) + \frac{\partial \vec{f}}{\partial \vec{v}}\left(\vec{v}^{n+1} - \vec{v}^{n}\right) \tag{3}$$

Following a method used in a study simulating the behavior of cloth [5], equations (2) and (3) can be combined and expressed as the linear system:

$$\left(I - \frac{2}{3}hM^{-1}\frac{\partial \vec{f}}{\partial \vec{v}} - \frac{4}{9}h^2M^{-1}\frac{\partial \vec{f}}{\partial \vec{x}}\right)\left(\vec{x}^{n+1} - \vec{x}^{n}\right) = \frac{1}{3}\left(\vec{x}^{n} - \vec{x}^{n-1}\right) + \frac{h}{9}\left(8\vec{v}^{n} - 2\vec{v}^{n-1}\right) + \frac{4}{9}h^2M^{-1}\left(\vec{f}^{n} - \frac{\partial \vec{f}}{\partial \vec{v}}\vec{v}^{n}\right) - \frac{2}{9}hM^{-1}\frac{\partial \vec{f}}{\partial \vec{v}}\left(\vec{x}^{n} - \vec{x}^{n-1}\right) \tag{4}$$

The Jacobian matrix expressing the partial derivative of the net force vector with respect to velocity is an N x N block matrix where N is the number of nodes in the system, and each block is 3 x 3. The forces due to translational and bending

springs as well as those due to applied pressure do not depend explicitly on nodal velocity, so their contributions are zero. Only the viscous damping term depends on nodal velocity, and its partial derivative yields $-bI$ where b is the damping coefficient and I is the $3N$ x $3N$ identity matrix.

The Jacobian matrix expressing the partial derivative of the net force vector with respect to position is the same size as the Jacobian considered above. In this case, the forces due to viscous damping and those due to applied pressure do not depend explicitly on position, so their contributions are zero. The forces due to the translational springs depend on nodal position, and their contribution to the Jacobian was evaluated analytically. For the translational spring between nodes i and j, elements of the Jacobian are computed as:

$$\frac{\partial \vec{f}_i}{\partial \vec{x}_i} = \frac{\partial \vec{f}_j}{\partial \vec{x}_j} = J \tag{5}$$

and

$$\frac{\partial \vec{f}_i}{\partial \vec{x}_j} = \frac{\partial \vec{f}_j}{\partial \vec{x}_i} = -J \tag{6}$$

where

$$J = \begin{pmatrix} l\left(r - s_x^{\,2}\right) - r^{3/2} & -ls_x s_y & -ls_x s_z \\ -ls_x s_y & l\left(r - s_y^{\,2}\right) - r^{3/2} & -ls_y s_z \\ -ls_x s_z & -ls_y s_z & l\left(r - s_z^{\,2}\right) - r^{3/2} \end{pmatrix} \tag{7}$$

In this equation, l is the undeformed length of the spring between nodes i and j, $\{s_x\ s_y\ s_z\}^{\mathrm{T}}$ is the vector from node i to node j, and $r = \{s_x\ s_y\ s_z\}*\{s_x\ s_y\ s_z\}^{\mathrm{T}}$.

The forces due to the bending springs also depend on nodal position. However, bending spring stiffness was about 5 orders of magnitude smaller than the translational spring stiffness, and it was assumed that the forces and their rates of change were also much less than those of the translational springs, making a negligible contribution to the total Jacobian.

2.3.3 Constraints

Zero-displacement boundary conditions as well as constraints imposed by chords that have reached their extension limit, are implemented through use of the inverse-mass matrix appearing in equation 4. A particle i acted upon by translational and bending springs but not subject to any displacement constraints will contribute the 3 x 3 diagonal matrix given by $(1/m_i)I$ to the main diagonal of the $3N$ x $3N$ inverse-mass matrix. However, we could prevent the velocity of the particle from changing by making the inverse-mass equal to zero, *i.e.*, giving the particle an infinite mass. An infinite mass cannot be accelerated, so it effectively ignores all forces exerted on it. The zero displacement boundary conditions at the mitral valve annulus and at nodes where chords terminate in the heart wall are handled this way in the model.

This approach can be extended to allow a node to ignore forces along certain directions [1]. To prevent a particle from accelerating in the direction given by unit vector p, we let that particle contribute $(1/m_i)(I\text{-}pp^T)$ to the main diagonal of the inverse-mass matrix. The leaflet nodes where chords attach are treated in this manner, where the unit vector p corresponds to the direction of the chord.

2.3.4 Integration method

Equation 4 is a linear system where the first term on the left side is a sparse $3N$ x $3N$ matrix and the second term is a $3N$ x 1 vector of unknowns. All of the terms on the right side are $3N$ x 1 vectors which are known. It can be solved by inverting the sparse matrix. We chose an iterative method to enable handling of meshes with a large number of nodes. The method of conjugate gradients is one the most efficient sparse matrix solvers but can only be used on symmetric matrices. Since the matrix is, in general, not symmetric due to the chord constraints in the inverse-mass matrix, we used a modified conjugate gradient method, which first multiplies the matrix by its transpose [2].

2.3.5 Collision handling

Potential self-collisions were identified using a spatial partitioning scheme. Potentially colliding triangles were then checked explicitly for triangle-triangle collision [4]. When the node of a triangle is determined to have broken the plane of another triangle, a force is applied to that node to balance the component of the net force at that node that lies in the direction of the surface normal.

2.3.6 Model parameters and implementation

Some of the model parameters, such as spring stiffnesses and applied transleaflet pressure, affect the closed shape of the valve at equilibrium. These parameters are assigned physically realistic values. The other model parameters affect model dynamics and/or stability, and those are assigned in order to minimize execution time and instability. See Table 1. The model was implemented in the Matlab programming language.

Table 1. Model parameters.

Parameter	Value
translational spring stiffness (normalized)	2 Nm/m
bending spring stiffness (normalized)	0.00002 Nm/rad
chord stiffness (normalized)	40 Nm/m
damping	1.0 N/(m/s)
leaflet thickness	1 mm
leaflet mass density	1.06 g/cc
applied transleaflet pressure	13 kPa (100 mmHg)

3. RESULTS

Figure 2, left panel, shows a volume rendering of the CT image showing the portion of the volume containing the mitral valve (oblique view from the top) in the opened position. Figure 2, center panel, shows the initial state of the mass-spring model of the valve from the same view. The chords are depicted by blue dashed lines. The model shown contains 277 nodes and 419 triangles, and consists of 701 translational springs and 579 bending springs. The largest stable integration time step that could be used was 30 μsec, and it took approximately 2000 steps to close the valve leaflets. Figure 2, right panel, shows the final state of the mass-spring model representing the closed mitral valve. The valve model closed completely in approximately 9 minutes on a computer with 2.33 GHz CPU and 2 GB of RAM.

While this model is probably adequate for surgical planning purposes, to fully ascertain the method's fidelity we also developed a higher-resolution model containing 716 nodes and 1239 triangles (1958 translational springs and 1775 bending springs). The largest stable integration time step for this model was 15 μsec, and it took approximately 30,000 steps to close the valve leaflets. Figure 3 shows a top view of the higher-resolution mitral valve model in both the open and closed positions. A surface produced from an image of the same valve in the closed position is also shown. The curve indicating where the valves “coapt”, or meet, is shown in red on both the closed model and the closed image for comparison.

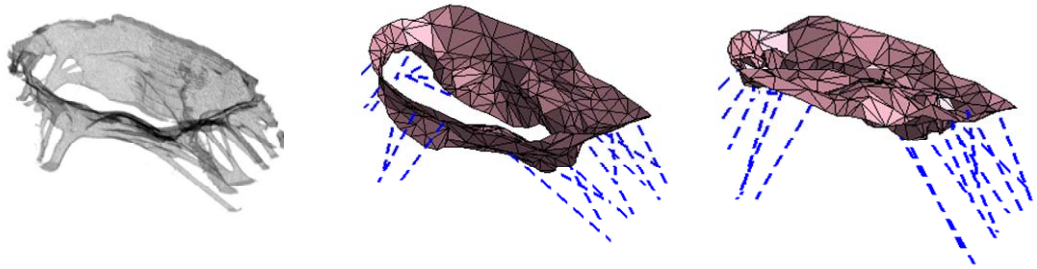

Figure 2. Left panel shows a CT image of the mitral valve in the open position. Center panel shows a low resolution model (277 nodes and 419 triangles) in the open position, with chords shown as dashed blue lines. Right panel shows the same model in the closed position.

To quantitatively compare the closed state predicted by the model (Figure 3, center) to the closed state generated from the image of the closed valve (Figure 3, right), the two surfaces were co-registered. This was done by selecting a paired sample of points on the annulus of each surface and then computing the translation vector and rotation matrix using a singular value decomposition approach [18]. The two co-registered surfaces are shown in Figure 4, left. The error in the closed state predicted by the model is estimated by computing the distances between points on the closed image and their nearest points on the closed model. This distance is mapped to color and is plotted in the right panel of Figure 4. The mean value of the error across the surface was 2.5 mm.

4. DISCUSSION

The goal of this study was to develop a simplified model of mitral valve mechanics specifically for use in surgical planning. There are three main requirements for the model. First, the geometry of the valve structures must be based directly on medical images. Second, the model must be able to simulate valve closure quickly (on the order of minutes). The third requirement concerns accuracy, and both the assumptions and parameter choices of the mass-spring model, as well as the initial geometry of the model mesh, affect accuracy. Each of these requirements will be discussed below.

We used micro-CT images of explanted hearts statically loaded with air to acquire mitral valve geometry. This method provided high resolution and contrast and enabled us to acquire images under carefully controlled loading conditions. Micro-CT scans cannot be used to acquire images in the clinical setting because of the small bore diameter, and a patient's heart cannot be statically loaded for imaging. However, flat-panel volume CT can be used to image a human heart *in vivo* with similar resolution to our data [12], and cardiac gating allows images to be captured at any point in the cardiac cycle, obviating the need for static loading. Our use of air to load the valve provided excellent contrast and allowed us to use very simple methods for segmenting the valve leaflets and chords. However, it is likely that valve tissues could be adequately segmented by introducing contrast agents to the blood and by using more sophisticated segmentation methods.

Our 277-node mitral valve model was able to simulate one closing cycle in just under 10 minutes. This is a little slower than desired; at that rate, it would take a surgeon several hours to simulate 10 or 12 surgical repair strategies. On the other hand, the model is implemented entirely in an interpreted prototyping language, and we have not yet made specific attempts to accelerate the simulations. For example, approximately 92% of the total execution time is spent assembling the vectors of nodal forces due to springs and applied pressure. These steps could not be vectorized but instead rely on loops. Converting these steps to the C programming language could speed up the simulations by as much as 10 times. Further gains could be made by taking advantage of multiple CPU's or even using the GPU.

In choosing mass-spring modeling over finite element approaches, we have deliberately traded off some accuracy in the interest of speed. Finite element methods are based on continuum mechanics and can handle the anisotropy and nonlinearity that are known to characterize valve biomechanics [17]. However, based on our experience both during surgery and in experiments with explanted hearts, the ability of the mitral valve to close effectively is primarily governed by gross geometric factors rather than by constitutive properties of the leaflets and chords. To be useful, our linear isotropic network of springs must only be able to predict whether a valve complex with given geometry will close realistically. To validate our model, we both qualitatively and quantitatively compare the closed state predicted by the model to the image of the closed valve.

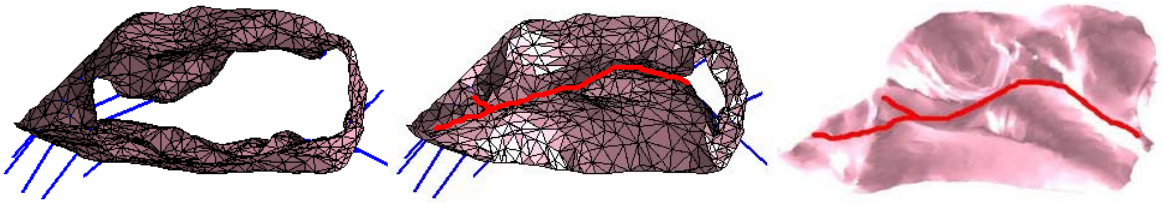

Figure 3. Left and center panels show a top view of the high resolution model of the mitral valve in the open and closed positions, respectively. Right panel shows the surface computed from an image of the same valve in the closed position. In both the model and the image of the closed valve, the line where the leaflets coapt (meet) has been drawn in red.

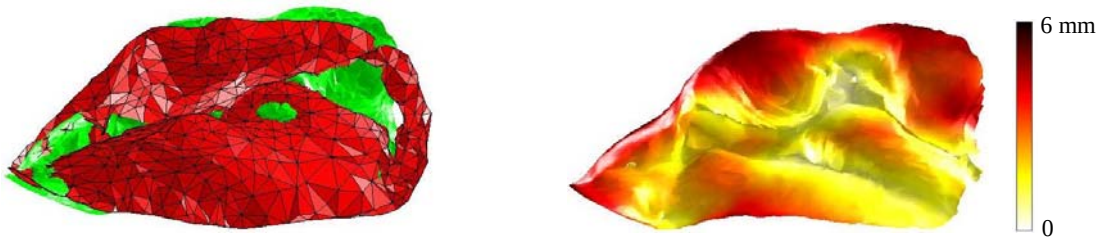

Figure 4. Left panel shows a top view of the closed valve leaflets. The model prediction is shown in dark red, and the surface generated from the image of the closed valve is shown in light green. The right panel shows the error in the closed state predicted by the model. For reference, the valve measures about 35 mm wide (in the left to right direction).

The main bulges and folds of the leaflet that were visible in the image of the closed valve were present in the model in the closed position, and the curve formed by the coaptation (meeting) of the leaflets was similar. However, in one region of the valve, the leaflets did not meet at all (Fig. 3, center panel). One possible cause could be that model chords restricted leaflet travel in that region. However, closure did not improve by deliberately lengthening the chords attached to that part of the leaflet. Another possibility is that the leaflet was folded/overlapped in that region in the original image so that a portion of the leaflet is not represented in the mesh of the open valve. Another potential reason is that the stiffness of the leaflet varies across its surface, due to local changes in thickness and/or material properties. Finally, our annular boundary conditions could be preventing the model leaflets from meeting in that region. We assume a fixed annulus, but the image of the closed valve shows that the annulus is pulled toward the center of the valve at the middle of the right edge (Fig3, right panel). This deformation of the annulus toward the center of the valve during valve closure might be critical for complete coaptation of the valve leaflets. In fact, Figure 3, right panel also shows that the annulus is pulled toward the center at the middle of the top and bottom edges too, and this could provide more leaflet surface in the coaptation region, potentially closing the gap.

By quantifying and plotting the error in the closed state predicted by the model, we can clearly see in which regions the model succeeds or fails to capture the actual behavior. In the lighter colored regions (white to yellow), error is less than about 2 millimeters indicating reasonably good model prediction. In darker regions (red to black), error is greater than about 4 mm, highlighting where model prediction is poor. The error surface in Figure 4, right panel, shows that error is small near the coaptation region of the leaflets and is large near the annulus. The region where the leaflets fail to close completely at the right side of the coaptation region is also visible, and, again, may be a manifestation of the poor fit at the annulus. Note that this poor fit at the annulus is not a problem with model dynamics because we defined the annular nodes from the image of the opened valve and constrained those nodes to zero displacement. Our results suggest that annular deformation must be considered, perhaps by moving the annular nodes to their positions in the closed state during the simulation.

Our method for simulating the mitral valve makes significant progress toward meeting the requirements of a surgical planning system. Model geometry is derived directly from medical images, simulating the closed state of the valve is rapid and has the potential to be sped up dramatically, and the model is able to predict many features of the closed state accurately, although it can be limited by the handling of boundary conditions.

ACKNOWLEDGEMENTS

D. Perrin is supported by NIH grant F32 HL084965-02.

REFERENCES

[1] Baraff, D. and Witkin, A. “Large steps in cloth simulation,” Computer Graphics, 43-54 (1998).

[2] Barrett, R., Berry, M., Chan, T.F., Demmel, J., Donato, J., Dongarra, J., Eijkhout, V., Pozo, R., Romine, C., Van der Vorst, H.

[Templates for the Solution of Linear Systems: Building Blocks for Iterative Methods, 2nd Edition], SIAM, Philadelphia, PA (1994).

[3] Bonow, R.O., Carabello, B.A., Chatterjee, K., de Leon, A.C. Jr., Faxon, D.P., Freed, M.D., Gaasch ,W.H., Lytle, B.W., Nishimura, R.A., O'Gara, P.T., O'Rourke, R.A., Otto, C.M., Shah, P.M., Shanewise, J.S. "Guidelines for the management of patients with valvular heart disease. A report of the American College of Cardiology/American Heart Association Task Force on Practice Guidelines (Writing Committee to Revise the 1998 Guidelines for the Management of Patients with Valvular Heart Disease)," Circ, 114(5), e1-e148 (2006).

[4] Bridson, R., Fedkiw, R., Anderson, J. "Robust treatment of collisions, contact, and friction for cloth animation," Computer Graphics, 594-603 (2002).

[5] Choi, K.J. and Ko, H.S. "Stable but responsive cloth," ACM Trans Graphics, 21(3), 604-611 (2002).

[6] Cosgrove, D. "View from North America's cardiac surgeons," Eur J Cardiothorac Surg, 26(1), S27-S31 (2004).

[7] Einstein, D.R., Kunzelman, K.S., Reinhall, P.G., Nicosia, M.A., Cochran, R.P. "Non-linear fluid-coupled computational model of the mitral valve," J Heart Valve Dis, 14, 376-385 (2005).

[8] Fuhrmann, A., Gross, C., Luckas, V. "Interactive animation of cloth using self collision detection," Journal of WECG, 11(1), 141-148 (2003).

[9] Gammie, J.S., O'Brien, S.M., Griffith, B.P., Ferguson, T.B., Peterson, E.D. "Influence of hospital procedural volume on care process and mortality for patients undergoing elective surgery for mitral regurgitation," Circ, 115, 881-887 (2007).

[10] Goldman, M.E., Mora, F., Guarino, T., Fuster, V., Mindich, B.P. "Mitral valvuloplasty is superior to valve replacement for preservation of left ventricular function: an intraoperative two-dimensional echocardiographic study," J Am Coll Cardiol, 10, 568–575 (1987).

[11] Gunderson, T.J., Nelson, T.B., Sullivan, A.J. [Heart valve market overview], US Bancorp Piper Jaffray, Minneapolis, MN (2003).

[12] Gupta, R., Grasruck, M., Suess, C., Bartling, S.H., Schmidt, B., Stierstorfer, K., Popescu, S., Brady, T., Flohr, T. "Ultra-high resolution flat-panel volume CT: fundamental principles, design architecture, and system characterization," Eur Radiol, 16, 1191–1205 (2006).

[13] Kunzelman, K.S., Cochran, R.P., Chuong, C., Ring, W.S., Verrier, E.D., Eberhart, R.D. "Finite element analysis of the mitral valve," J Heart Valve Dis, 2, 326-340 (1993).

[14] Lim, K.H., Yeo, J.H., Duran, C.M. "Three-dimensional asymmetrical modeling of the mitral valve: a finite element study with dynamic boundaries," J Heart Valve Dis, 14, 386-392 (2005).

[15] Moss, R.R., Humphries, K.H., Gao, M., Thompson, C.R., Abel, J.G., Fradet, G., Munt, B.I. "Outcome of mitral valve repair or replacement: a comparison by propensity score analysis," Circ, 108 suppl II, II90-II97 (2003).

[16] Ng, H.N. and Grimsdale, R.L. "Computer Graphics Techniques for Modeling Cloth," IEEE Computer Graphics and Applications, 16(5), 28-41 (1996).

[17] Sacks, M.S., Enomoto, Y., Graybill, J.R., Merryman, W.D., Zeeshan, A., Yoganathan, A.P., Levy, R.J., Gorman, R.C., Gorman, J.H. "In-vivo dynamic deformation of the mitral valve anterior leaflet," AnnThorac Surg, 82, 1369-1378 (2006).

[18] Strang, G. [Introduction to Linear Algebra, 2nd edition], Wellesley-Cambridge Press, Wellesley, MA, Chapter 7 (1998).

[19] Tischler, M.D., Cooper, K.A., Rowen, M., LeWinter, M.M. "Mitral valve replacement versus mitral valve repair: a Doppler and quantitative stress echocardiographic study," Circ, 89, 132–137 (1994).

[20] Votta, E., Maisano, F., Bolling, S.F., Alfieri, O., Montevecchi, F.M., Redaelli, A. "The Geoform disease-specific annuloplasty system: A finite element study," Ann Thorac Surg, 84, 92–102 (2007).